Available online at www.sciencedirect.com
SCIENCE DIRECT®
Optics & Laser Technology 37 (2005) 337–344
Optics & Laser Technology
www.elsevier.com/locate/optlastec

Parameter optimization and characteristic analysis of a polymer microring resonant wavelength multiplexer

Xian-Yin Wang[a,b], Chun-Sheng Ma[a,*], Shu-Lin E[b], Xin Yan[a], Yuan-Zhe Xu[a], Hai-Ming Zhang[a], Da-Ming Zhang[a], Zhan-Chen Cui[c], De-Gui Sun[b]

[a] *State Key Laboratory on Integrated Optoelectronics, College of Electronic Science and Engineering, Jilin University, 119 Jiefang Road, Changchun 130023, China*

[b] *State Key Laboratory on Applied Optics, Changchun Institute of Optics, Fine Mechanics and Physics, Chinese Academy of Sciences, Changchun 130021, China*

[c] *College of Chemistry, Jilin University, Changchun 130023, China*

Received 4 November 2003; accepted 22 April 2004

Available online 23 July 2004

Abstract

Novel formulas of transmission functions are presented, some parameters are optimized, and transmission characteristics are analyzed for a polymer microring resonant wavelength multiplexer around the central wavelength of 1.55 μm with the wavelength spacing of 5.6 nm and with eight vertical output channels. The computed results show that the designed device possesses some excellent features including the 3 dB bandwidth of 0.25 μm, weaker background light of 3.8×10^{-4}, smaller inserted loss of less than 0.6 dB, and lower crosstalk below −20 dB for every vertical output channel.

Keywords: Polymer; Microring resonance; Wavelength multiplexer; Transmission spectrum; Inserted loss; Crosstalk

1. Introduction

The wavelength multiplexer composed of some microring resonator elements is a novel device in optical telecommunication systems. In the last decade, various kinds of microring resonators [1–5] for integrated optics have received considerable attention because of some excellent features, such as lower inserted loss, smaller crosstalk, and easier integration of fabrication. Recently, some researchers have designed and fabricated some microring resonant wavelength multiplexer which exhibited good wavelength demultiplexing in experiments [6,7].

Electro-optic polymers can also be used to fabricate wavelength multiplexers, which possess better thermal stability and temperature dependence, smaller birefringence, and easier control of the refractive index. Therefore, polymers are promising materials for fabricating multiplexers including arrayed waveguide gratings (AWG) and microring resonators (MRR).

In this paper, in order to obtain better wavelength demultiplexing, first we perform the optimization for the parameters of a polymer microring resonant wavelength multiplexer. Then we present novel formulas of transmission functions, and use them to analyze the transmission characteristics of this kind of device around the central wavelength of 1.55 μm with the wavelength spacing of 5.6 nm and with 8 vertical output channels. Finally, we reach some conclusions on the basis of the analysis and discussion.

2. Parameter optimization

In order to obtain the better wavelength demultiplexing, in this section, the values of some parameters of the polymer microring resonant wavelength multiplexer for the E_{00}^{x} mode are optimized.

2.1. Structure of the device

Fig. 1(a) shows the schematic diagram of a polymer microring resonant wavelength multiplexer with eight

*Corresponding author. Tel.: +86-431-8923189-2476; fax: 0086-431-8964939.

E-mail addresses: mcsheng@163.com, guo0124@263.net (C.-S. Ma).

0030-3992/$ - see front matter © 2004 Elsevier Ltd. All rights reserved.
doi:10.1016/j.optlastec.2004.04.016

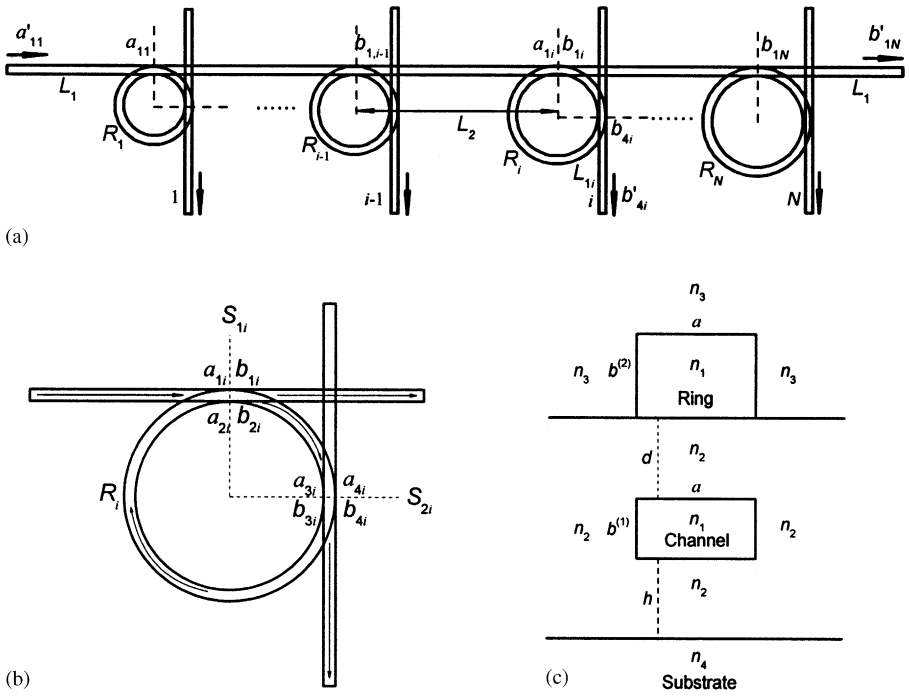

Fig. 1. (a) Schematic diagram of a microring resonant wavelength multiplexer, (b) that of a basic filter element, and (c) cross sections and refractive index profiles of the channel and the microring.

vertical output channels. Every polymer microring is placed on the top of the main polymer channel and the corresponding polymer vertical output channel which are buried in another polymer cladding on the Si substrate. Assume that the total length of the main channel is $2L_1 + (N-1)L_2$, where L_1 is the distance from the input or output port of the main channel to the adjacent coupling point, and L_2 is that of the adjacent coupling points on the main channel, L_{1i} is that from the output port of the ith vertical channel to the adjacent coupling point. Fig. 1(b) shows a basic filter element, and Fig. 1(c) shows the cross sections and the refractive index profiles of the channel and the microring, which have the same core width a and different core thickness $b^{(1)}$ and $b^{(2)}$, and have the same core refractive index n_1 and different cladding indices n_2 and n_3, respectively. Selecting the proper values of the material and structural parameters, we can control the channels and the microrings to have the same mode propagation constant.

In the following analysis, the values of parameters used in the calculation are given in the relative figure captions.

2.2. Size of the vertical channels and rings

Fig. 2 presents the curves of the effective refractive indices n_c versus the core thickness $b^{(1)}$ and $b^{(2)}$ of the channel and the microring, respectively, which are solved from the eigenvalue equations of the E^x_{pq} mode

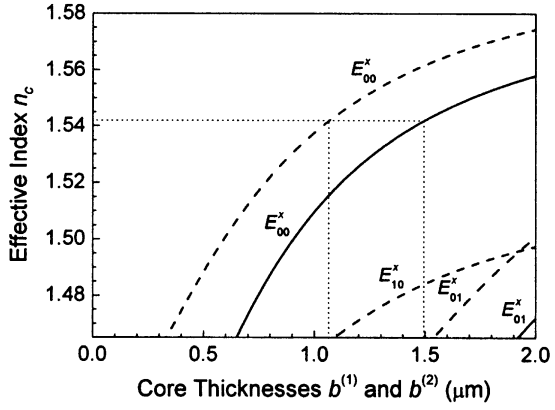

Fig. 2. Curves of n_c versus $b^{(1)}$ (dashed lines) and $b^{(2)}$ (solid lines) for E^x_{pq} mode, where $a = 2$ μm, $\lambda = 1.550918$ μm, $n_1 = 1.6278, n_2 = 1.465, n_3 = 1$.

of the rectangular optical waveguide [8]. We can find that when we select the core width and thicknesses of channels and microrings to be $a = 2.0$ μm, $b^{(1)} = 1.07$ μm and $b^{(2)} = 1.5$ μm, respectively, the single mode propagation is realized in the device, and both the channel and the microring have the same propagation constant.

Fig. 3 presents the curves of the effective refractive indices n_c versus the propagating wavelength λ for the channel and the microring, respectively. We can also find that the device has also realized single mode

propagation in the range of 1.53 to 1.58 μm, which has covered all the eight resonant wavelengths of the device.

2.3. Amplitude coupling ratio

Fig. 4 shows the relation between the amplitude coupling ratio κ and the thickness d of the coupling layer between the microring and the channel, which is calculated from the mode coupling theory [9]. It can be seen that the amplitude coupling ratio κ can be limited in the range 0.1–0.3 when the thickness of the coupling layer d is varied form 0.85 to 0.4 μm.

2.4. Resonant order, radii of microrings, radius difference of adjacent rings, free spectrum range (FSR), and the maximum number of channels in a FSR

Assume that the wavelengths of the N signals input from the input port of the main channel are $\lambda_i = \lambda_1 + (i-1)\Delta\lambda$, where λ_1 is the initial wavelength and $\Delta\lambda$ is the wavelength spacing, and the relative resonant radii of the N microrings are $R_i = R_1 + (i-1)\Delta R$, where R_1 is the initial radius, and ΔR is the radius difference of adjacent microrings. Let m be the resonant order, according to the following resonant equation of the microring [10–12].

$$2\pi R_i n_c = m\lambda_i, \tag{1}$$

the equations of the resonant radius of the central microring R, group refractive index n_g, radius difference of adjacent microrings ΔR, free spectral range FSR, and the maximum number of the vertical output channels in a FSR is

$$R = \frac{m\lambda}{2\pi n_c}, \tag{2}$$

$$n_g = n_c - \lambda\frac{dn_c}{d\lambda}, \tag{3}$$

$$\Delta R = \frac{dR}{d\lambda}\Delta\lambda = \frac{mn_g}{2\pi n_c^2}\Delta\lambda, \tag{4}$$

$$\mathrm{FSR} = \frac{\lambda}{m}\frac{n_c}{n_g}, \tag{5}$$

$$N_{max} = \mathrm{int}\left(\frac{\mathrm{FSR}}{\Delta\lambda}\right) = \mathrm{int}\left(\frac{\lambda}{m\Delta\lambda}\frac{n_c}{n_g}\right). \tag{6}$$

Fig. 5 shows the relations between the resonant order m and R, ΔR, FSR and N_{max}. It is found that a proper value should be elected for m. If m is too large, FSR and N_{max} would be too small, it would be uneasy to realize the demultiplexing of the device. On the other hand, if m is too small, R and ΔR would be too small, this would cause larger bent loss of the microrings, and it would be difficult to fabricate the device. A larger wavelength spacing $\Delta\lambda$ leads to a larger radius difference ΔR, therefore, we had to choose a larger wavelength spacing $\Delta\lambda$ to produce a larger radius difference ΔR, which would benefit the fabrication of this kind of wavelength multiplexer. Considering the conditions of our laboratory and the practical structure of the device, for the

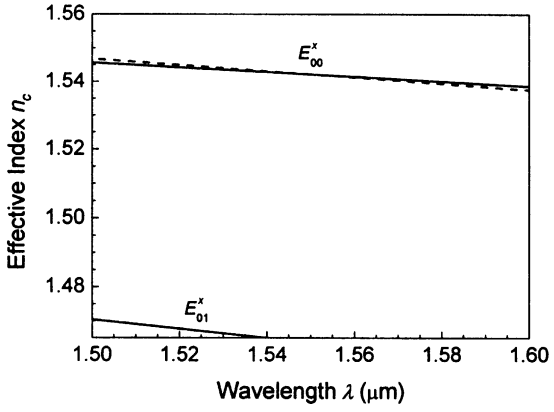

Fig. 3. Curves of n_c versus λ for E_{pq}^x mode, where the values of parameters are the same as those of Fig. 2, solid lines are for the channel, dashed line is for the microring.

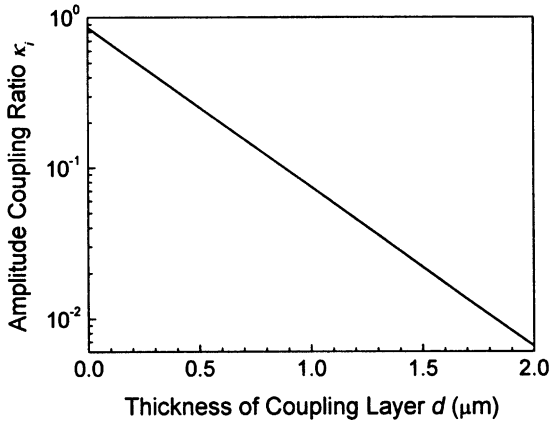

Fig. 4. Curves of κ_i versus d for E_{00}^x mode, where the values of parameters are the same as those of Fig. 2.

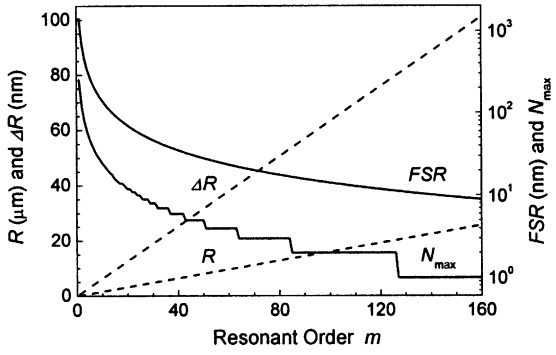

Fig. 5. Curves of $R, \Delta R$, FSR and N_{max} versus m, where $a = 2.0$ μm, $b^{(2)} = 1.5$ μm, $\lambda = 1.550918$ μm, $\Delta\lambda = 5.6$ nm, $n_1 = 1.6278$, $n_2 = 1.465$, $n_3 = 1$.

Table 1
Optimum values of parameters of the polymer device for the E_{00}^{x} mode

Central wavelength	$\lambda = 1.550918$ μm
Wavelength spacing	$\Delta\lambda = 5.6$ nm
Refractive index of polymer core of channels and microrings	$n_1 = 1.6278$
Refractive index of polymer claddings of channels	$n_2 = 1.465$
Refractive index of air claddings of microrings	$n_3 = 1$
Core width of channels and microrings	$a = 2$ μm
Core thickness of channels	$b^{(1)} = 1.07$ μm
Core thickness of microrings	$b^{(2)} = 1.5$ μm
Thickness of the coupling layer between channels and microrings	$0.4 \leqslant d \leqslant 0.85$ μm
Amplitude coupling ratio	$0.3 > \kappa_i > 0.1$
Resonant order	$m = 79$
Microring radius for central wavelength	$R = 12.65$ μm
Radius difference of adjacent microrings	$\Delta R = 50.0$ nm
Free spectral range	FSR = 18.0 nm
Maximum number of vertical output channels in a FSR	$N_{max} = 3$
Total number of vertical output channels	$N = 8$

central wavelength of 1.550918 μm, we select $m = 79$ and $\Delta\lambda = 5.6$ nm to achieve a resonant radius of 12.645 μm, a radius increment of 50 nm, and a FSR of 18 nm. In the design, eight wavelengths are inserted in three adjacent FSRs.

The optimum values of parameters of the device are listed in Table 1.

3. Characteristic analysis

In this section, the characteristics of the polymer microring resonant wavelength multiplexer designed above are analyzed, which include the bent loss of the microrings, leakage loss caused by the substrate with higher refractive index, transmission spectrum, inserted loss and crosstalk of every vertical output channel.

3.1. Bent loss of the microring

The inserted loss of the device includes the mode scatter loss mainly caused by the roughness of the interfaces of the waveguides, bent loss of the microrings, leakage loss resulted from the high refractive index substrate, and propagation loss due to the absorption of the materials of the device. The mode scatter loss can be disregarded by dint of the improvement of fabrication technology. Therefore, we only care about the effects of the above bent loss, leakage loss and propagation loss on the transmission characteristics of the device.

Fig. 6 plots the curves of the bent loss coefficient $2\alpha_b$ versus the bent radius R, which is calculated from the formula presented in Ref. [13]. It is found that the bent loss coefficient $2\alpha_b$ decreases as the bent radius R increases. To be precise, $2\alpha_b$ is dropped down to 2.0×10^{-3}/cm for the bent radius R being 12.65 μm, which is much smaller compared to the propagation loss coefficient $2\alpha_p$ which is taken to be 0.1/cm.

3.2. Leakage loss caused by the substrate

The channels and the microrings are formed on the Si substrate which possesses a higher refractive index of $n_4 = 3.45$ compared with that of the guide core of $n_1 = 1.6278$.

Fig. 7 plots the curves of the leakage loss coefficient $2\alpha_l$ versus the thickness h of the confined layer between the guide core and the substrate, which is calculated from the formula presented in Ref. [14]. It is found that the leakage loss coefficient $2\alpha_l$ decreases as the confined layer thickness h increases. To be precise, $2\alpha_l$ is dropped down below 10^{-9}/cm when the confined layer thickness h is larger than 6 μm, which is so small and can be neglected. Therefore, in the following analysis we only take account of the bent loss of the microrings and the

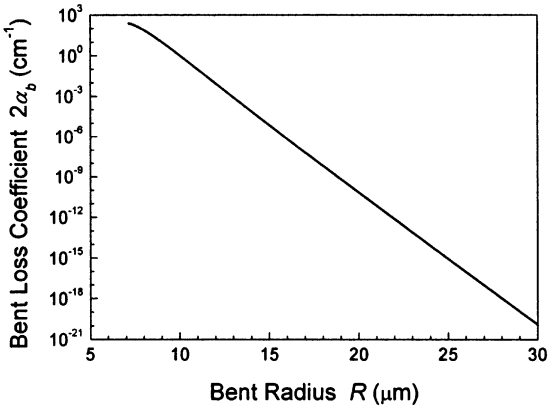

Fig. 6. Curves of $2\alpha_b$ versus R, where the values of parameters are the same as those of Fig. 5.

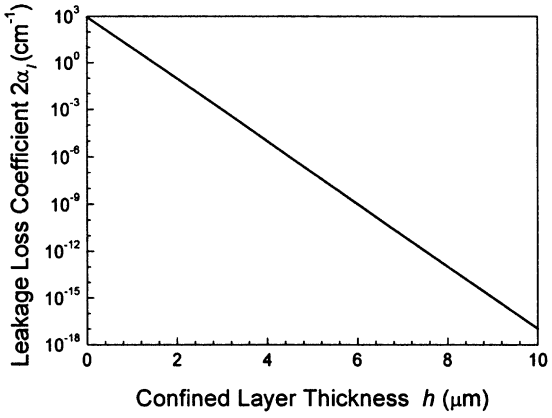

Fig. 7. Leakage loss of substrate $2\alpha_l$ versus h, where $a = 2.0$ μm, $b^{(1)} = 1.07$ μm, $\lambda = 1.550918$ μm, $n_1 = 1.6278$, $n_2 = 1.465$, $n_4 = 3.45$.

propagation loss in the channels and the microrings, and take $2\alpha_p$ to be 0.1/cm.

3.3. Transmission spectra

The transmission spectrum, inserted loss and crosstalk are important characteristics, which can judge the quality of a microring resonant multiplexer. In order to analyze these characteristics, we derive the transmission functions from the input port to the output port of the main channel B_N and that to the output port of the ith vertical channel D_i as follows, respectively (see the appendix)

$$|B_N|^2 = \left| \left(\prod_{i=1}^{N} U_i \right) \exp[-\mathrm{j}(N-1)\psi_2] \exp(-\mathrm{j}2\psi_1) \right|^2, \quad (7)$$

$$|D_i|^2 = \left| \left(\prod_{k=1}^{i-1} U_k \right) V_i \exp[-\mathrm{j}(i-1)\psi_2] \times \exp[-\mathrm{j}(\psi_{1i} + \psi_1)] \right|^2 \quad (i = 1, 2, \ldots, N), \quad (8)$$

with

$$U_i = \frac{t_i\{1 - \exp[-\mathrm{j}(\phi_{1i} + \phi_{2i})]\}}{1 - t_i^2 \exp[-\mathrm{j}(\phi_{1i} + \phi_{2i})]}, \quad (9)$$

$$V_i = -\frac{\kappa_i^2 \exp(-\mathrm{j}\phi_{2i})}{1 - t_i^2 \exp[-\mathrm{j}(\phi_{1i} + \phi_{2i})]}, \quad (10)$$

$$\psi_1 = L_1(\beta - \mathrm{j}\alpha_L), \qquad \psi_{1i} = L_{1i}(\beta - \mathrm{j}\alpha_L), \quad (11)$$

$$\psi_2 = L_2(\beta - \mathrm{j}\alpha_L), \quad (12)$$

$$\phi_{1i} = 3\pi R_i(\beta - \mathrm{j}\alpha_{Ri})/2, \qquad \phi_{2i} = \pi R_i(\beta - \mathrm{j}\alpha_{Ri})/2, \quad (13)$$

where, κ_i is the amplitude coupling ratio, $t_i = (1 - \kappa_i^2)^{1/2}$, β is the propagation constant of the channels and the microrings, $\alpha_L = \alpha_p$ is the propagation loss coefficient of the channels, $\alpha_{Ri} = \alpha_{bi} + \alpha_p$ is that of the ith microring which includes the bent loss and the propagation loss.

Fig. 8 shows (a) the transmission spectra in the range of more than two FSRs, and (b) those around the eight resonant wavelengths. Because this device is designed without periodicity, only those resonant wavelength labeled by λ_i $(i = 1, 2, \ldots, 8)$ in Fig. 8(a) can be output from the relative vertical channels, and the wavelength demultiplexing is realized in the device. The FSR of every filter element determined by the transmission function is consistent with that calculated by Eq. (5). We insert eight resonant wavelengths in three adjacent FSRs in the design of the device. We find that as the amplitude coupling ratio κ_i increases, the resonant peaks become wide, while the background light becomes strong. When we take $\kappa_i = 0.1, 0.2, 0.3$, the relative 3 dB bandwidth of the resonant peak is about 0.07, 0.25, 0.56 nm, and the relative minimum background light is dropped down to 2.3×10^{-5}, 3.8×10^{-4}, 2.1×10^{-3}, respectively.

3.4. Inserted loss

The inserted loss of every vertical output channel is defined as

$$L^{(i)}(\mathrm{dB}) = -10 \log_{10}(|D_i|^2), \quad (i = 1, 2, \ldots, N). \quad (14)$$

Fig. 9 shows the inserted loss of 8 vertical output channels. We find that as the resonant wavelength λ_i increases, the inserted loss also increases. When we take $\kappa_i = 0.1, 0.2, 0.3$, the inserted loss of every vertical output channel is dropped below 0.77, 0.57, 0.77 dB, respectively.

3.5. Crosstalk

The crosstalk of every vertical output channel is defined as

$$L_{CT}(\lambda_i)(\mathrm{dB}) = 10 \log_{10}\left(\frac{\sum_{j \neq i, j=1}^{N} |D_j|^2(\lambda_i)}{|D_i|^2(\lambda_i)} \right), \quad (i = 1, 2, \ldots, N). \quad (15)$$

Fig. 10 shows the crosstalk of 8 vertical output channels. We find that as the resonant wavelength λ_i increases, the crosstalk also increases. Additionally, larger power coupling ratio would cause larger cross talk. When we take $\kappa_i = 0.1, 0.2, 0.3$, the crosstalk of every vertical output channel is dropped below -30, -20, -10.5 dB, respectively.

4. Conclusion

On the basis of the above analysis and discussion of the polymer microring resonant wavelength multiplexer designed in this paper, some conclusion are reached as follows.

1. The resonant order of 79 and the wavelength spacing of 5.6 nm for the central wavelength about 1.55 μm is used to achieve a resonant radius of 12.645 μm and a radius increment of 50 nm, and lead to a FSR of 18 nm. The bent loss coefficient results from this radius of 12.645 μm is about 6×10^{-5}/cm, and it is smaller. Therefore, the inserted loss of the device is mainly caused by the propagation loss. Also, the radius increment of 50 nm can be realized in the fabrication of the device by the technology of our laboratory. The FSR of 18 nm contains three resonant wavelengths, so the 8 resonant wavelengths designed is inserted in three adjacent FSRs.

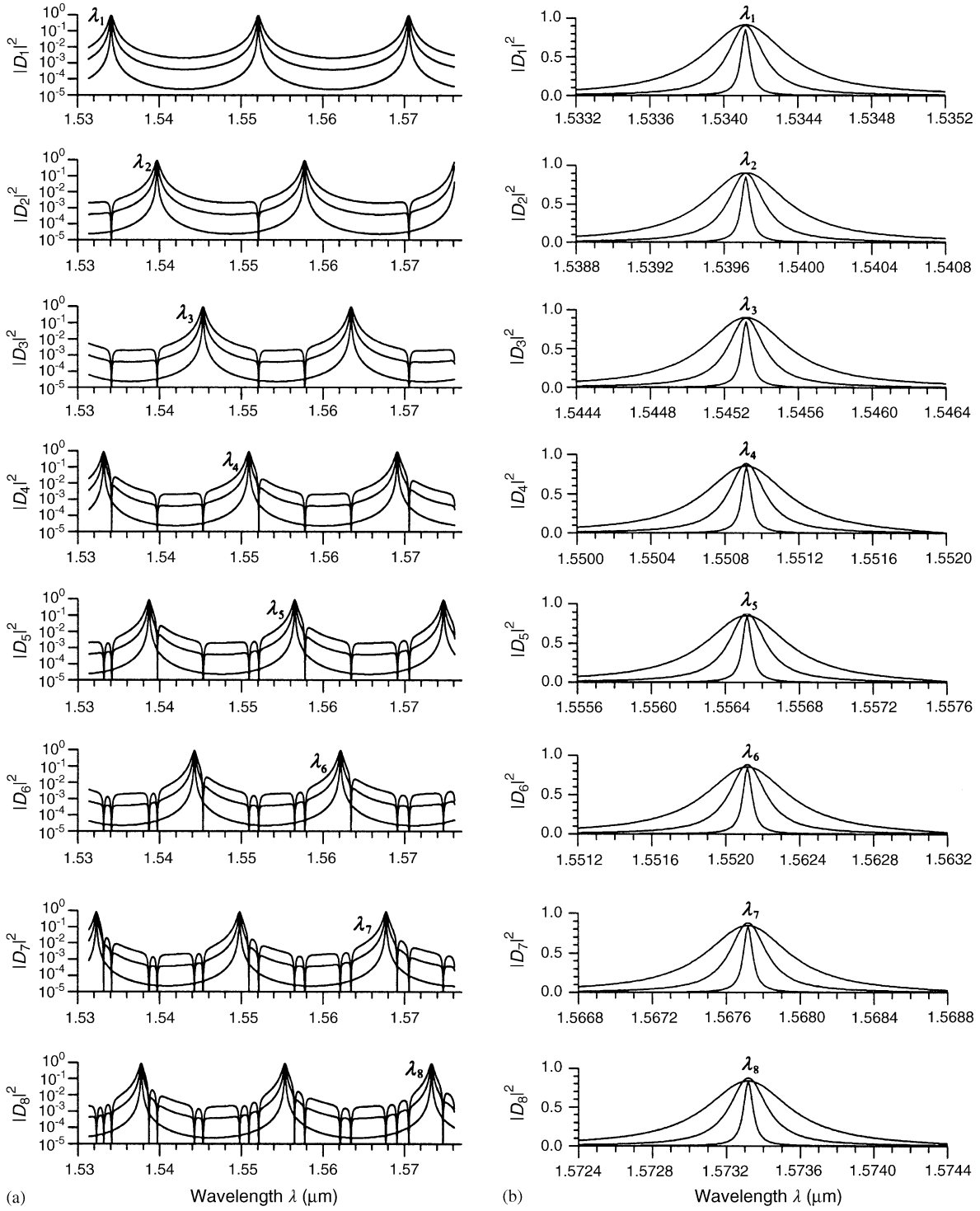

Fig. 8. (a) Transmission spectra in more than 2 FSRs, and (b) those around resonant wavelengths of eight vertical output channels, where $\Delta\lambda = 5.6$ nm, $\lambda_1 = 1.534118$ μm, $\lambda_2 = 1.539718$ μm, $\lambda_3 = 1.545318$ μm, $\lambda_4 = 1.550918$ μm, $\lambda_5 = 1.556518$ μm, $\lambda_6 = 1.562118$ μm, $\lambda_7 = 1.567718$ μm, $\lambda_8 = 1.573318$ μm; $\Delta R = 50.0$ nm, $R_1 = 12.50$ μm, $R_2 = 12.55$ μm, $R_3 = 12.60$ μm, $R_4 = 12.65$ μm, $R_5 = 12.70$ μm, $R_6 = 12.75$ μm, $R_7 = 12.80$ μm, $R_8 = 12.85$ μm; $L_1 = 4000$ μm, $L_2 = 100$ μm, $2\alpha_p = 0.1/\text{cm}$, $\kappa_i = 0.1, 0.2, 0.3$ corresponds to the three curves from the bottom to the top in every figure, the values of other parameters are the same as those of Fig. 5.

2. The analytical results by using the formulas of the transmission functions presented in this paper shows that the device designed has realized better wavelength demultiplexing in theory. In addition, taking the amplitude coupling ratio of 0.2, this device possesses some excellent features, such as the 3 dB bandwidth of

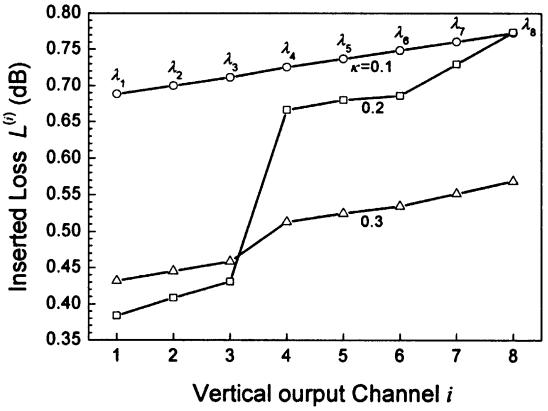

Fig. 9. Inserted loss of eight vertical channels, where the values of parameters are the same as those of Fig. 8.

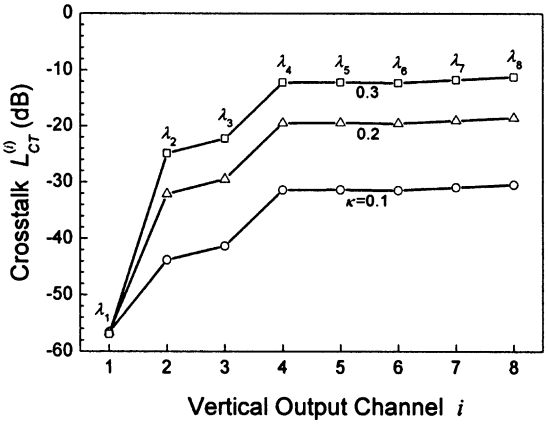

Fig. 10. Crosstalk of eight vertical channels, where the values of parameters are the same as those of Fig. 8.

0.25 μm, the weaker background light of 3.8×10^{-4}, smaller inserted loss less than 0.6 dB, and lower crosstalk below −20 dB for every output channel.

We think that this work would also be suitable and helpful for the design of some other similar microring resonant wavelength multiplexer. Currently this kind of polymer microring resonant wavelength multiplexer is being fabricated in our laboratory.

Acknowledgements

The authors wish to express their gratitude to the National Science Foundation Council of China and the Chinese Academy of Sciences (One Hundred Talent Project) for their generous support of this work.

Appendix

Let $a_{1i}, b_{1i}, a_{2i}, b_{2i}, a_{3i}, b_{3i}, a_{4i}, b_{4i}$ be the input and output amplitudes of the ith wavelength passing through the interfaces S_{1i} and S_{2i} in the ith filter element as shown in Fig. 1(b). By using $a_{2i} = b_{3i}\exp(-j\phi_{1i})$ and $a_{3i} = b_{2i}\exp(-j\phi_{2i})$, the following coupling equations can be obtained:

$$b_{1i} = t_i a_{1i} - j\kappa_i a_{2i} = t_i a_{1i} - j\kappa_i b_{3i}\exp(-j\phi_{1i}), \quad (A.1)$$

$$b_{2i} = -j\kappa_i a_{1i} + t_i a_{2i} = -j\kappa_i a_{1i} + t_i b_{3i}\exp(-j\phi_{1i}), \quad (A.2)$$

$$b_{3i} = t_i a_{3i} = t_i b_{2i}\exp(-j\phi_{2i}), \quad (A.3)$$

$$b_{4i} = -j\kappa_i a_{3i} = -j\kappa_i b_{2i}\exp(-j\phi_{2i}), \quad (A.4)$$

where the expressions of ϕ_{1i} and ϕ_{2i} are given by Eq. (13). Solving Eqs. (A.1)–(A.4), we have

$$b_{1i} = U_i a_{1i}, \qquad b_{4i} = V_i a_{1i}, \quad (A.5)$$

where the expressions of U_i and V_i are given by Eqs. (9) and(10), respectively. Substituting $a_{1i} = b_{1,i-1}\exp(-j\psi_2)$ into Eq. (A.5), we can derive the recurrence relations between amplitudes a_{1i} and b_{1i}, b_{4i} as follows

$$b_{11} = U_1 a_{11}, \qquad b_{41} = V_1 a_{11}, \quad (A.6)$$

$$b_{1i} = U_i b_{1,i-1}\exp(-j\psi_2), \qquad b_{4i} = V_i b_{1,i-1}\exp(-j\psi_2), \quad (i = 2, 3, \ldots, N) \quad (A.7)$$

From Eqs. (A.6) and (A.7) we obtain

$$\frac{b_{1N}}{a_{11}} = \left(\prod_{i=1}^{N} U_i\right)\exp[-j(N-1)\psi_2], \quad (A.8)$$

$$\frac{b_{4i}}{a_{11}} = \left(\prod_{k=1}^{i-1} U_k\right) V_i \exp[-j(i-1)\psi_2], \quad (i = 1, 2, \ldots, N). \quad (A.9)$$

By using $a'_{11} = a_{11}\exp(j\psi_1)$ and $b'_{1N} = b_{1N}\exp(-j\psi_1)$, B_N and D_N can be expressed as, respectively

$$B_N = \left|\frac{b'_{1N}}{a'_{11}}\right| = \left|\frac{b_{1N}}{a_{11}}\exp(-j2\psi_1)\right|, \quad (A.10)$$

$$D_i = \left|\frac{b'_{4i}}{a'_{11}}\right| = \left|\frac{b_{4i}}{a_{11}}\exp[-j(\psi_{1i} + \psi_1)]\right|, \quad (i = 1, 2, \ldots, N). \quad (A.11)$$

Substituting Eq. (A.8) into Eq. (A.10), Eq. (7) is obtained. Similarly, substituting Eq. (A.9) into Eq. (A.11), Eq. (8) is obtained.

References

[1] Little BE, Chu ST, Haus HA, Foresi JS, Laine JP. Microring resonator channel dropping filters. J Lightwave Technol 1997;15(6):998–1005.

[2] Little BE, Foresi JS, Steinmeyer G, Thoen ER, Chu ST, Haus HA, Ippen EP, Kimerling LC, Greene W. Ultra-compact Si–SiO_2 microring resonator optical channel dropping filters. IEEE Photon Technol Lett 1998;10(4):549–51.

[3] Chu ST, Little BE, Pan W, Kaneko T, Kokubun Y. Second-order filter response from parrel coupled glass microring resonators. IEEE Photon Technol Lett 1999;11(11):1426–8.
[4] Melloni A, Martinelli M. Synthesis of direct-coupled-resonators bandpass filters for WDM systems. J Lightwave Technol 2002;20(2):296–303.
[5] Gheorma IL, Osgood RM. Fundamental limitations of optical resonator based high-speed EO modulators. IEEE Photon Technol Lett 2002;14(6):795–7.
[6] Chu ST, Little BE, Pan W, Kaneko T, Sato S, Kokubun Y. An eight-channel add-drop filter using vertically coupled microring resonators over a cross grid. IEEE Photon Technol Lett 1999;11(6):691–3.
[7] Suzuki S, Hatakeyama Y, Kokubun Y, Chu ST. Precise control of wavelength channel spacing of microring resonator add-drop filter array. J Lightwave Technol 2002;20(4):745–9.
[8] Marcatili EAJ. Dielectric rectangular waveguide and directional coupler for integrated optics. Bell System Technol J 1969;48(7): 2071–102.
[9] Haus HA, Huang WP, Kawakami S, Whitaker NA. Coupled-mode theory of optical waveguides. J Lightwave Technol 1987;LT-5(1):16–23.
[10] Suzuki S, Oda K, Hibinio Y. Integrated-optic double-ring resonators with a wide free spectral range of 100 GHz. J Lightwave Technol 1995;13(8):1766–71.
[11] Kominato T, Ohmori Y, Takato N, Okazaki H, Yasu M. Ring resonators composed of GeO_2-doped silica waveguides. J Lightwave Technol 1992;10(12):1781–7.
[12] Oda K, Takato N, Toba H. A wide-FSR waveguide double-ring resonator for optical FDM transmission systems. J Lightwave Technol 1991;9(6):728–36.
[13] Marcatili EAJ. Bends in optical dielectric guides. Bell System Technol J 1969;48(7):2103–32.
[14] Suematsu Y, Furuya K. Quasi-guided modes and related radiation losses in optical dielectric waveguides with external higher index surroundings. IEEE Trans Microwave Theory Technol 1975;MTT-23(1):170–5.